Neuropharmacology 196 (2021) 108718

Contents lists available at ScienceDirect

Neuropharmacology

journal homepage: www.elsevier.com/locate/neuropharm

Biophysical and synaptic properties of NMDA receptors in the lateral habenula

Alvaro Nuno-Perez [a,**], Sarah Mondoloni [a], Anna Tchenio [a], Salvatore Lecca [a], Manuel Mameli [a,b,*,1]

[a] The Department of Fundamental Neuroscience, The University of Lausanne, 1005, Lausanne, Switzerland
[b] Inserm, UMR-S 839, 75005, Paris, France

ARTICLE INFO

Keywords:
Lateral habenula
Long-term potentiation
NMDA receptors
Subunit composition

ABSTRACT

Excitatory synaptic transmission in the lateral habenula (LHb), an evolutionarily ancient subcortical structure, encodes aversive stimuli and affective states. Habenular glutamatergic synapses contribute to these processes partly through the activation of AMPA receptors. Yet, N-methyl-D-aspartate receptors (NMDARs) are also expressed in the LHb and support the emergence of depressive symptoms. Indeed, local NMDAR blockade in the LHb rescues anhedonia and behavioral despair in rodent models of depression. However, the subunit composition and biophysical properties of habenular NMDARs remain unknown, thereby hindering their study in the context of mental health. Here, we performed electrophysiological recordings and optogenetic-assisted circuit mapping in mice, to study pharmacologically-isolated NMDAR currents in LHb neurons that receive innervation from different brain regions (entopeduncular nucleus, lateral hypothalamic area, bed nucleus of the stria terminalis, or ventral tegmental area). This systematic approach revealed that habenular NMDAR currents are sensitive to TCN and ifenprodil – drugs that specifically inhibit GluN2A- and GluN2B-containing NMDARs, respectively. Whilst these pharmacological effects were consistently observed across inputs, we detected region-specific differences in the current-voltage relationship and decay time of NMDAR currents. Finally, inspired by the firing of LHb neurons *in vivo*, we designed a burst protocol capable of eliciting calcium-dependent long-term potentiation of habenular NMDAR transmission *ex vivo*. Altogether, we define basic biophysical and synaptic properties of NMDARs in LHb neurons, opening new avenues for studying their plasticity processes in physiological as well as pathological contexts.

1. Introduction

The lateral habenula (LHb) is a phylogenetically conserved structure identified in virtually all vertebrate species (Bianco and Wilson, 2009). The widespread interest in this structure is based on the fact that LHb neurons control the firing activity of dopamine neurons of the ventral tegmental area (VTA), and serotonin neurons of the raphe nuclei (Clerke et al., 2021; Matsumoto and Hikosaka, 2007; Stern et al., 1979). LHb neurons present diversity in their genetic program. The vast majority are glutamatergic and long-range projecting, although a small proportion of LHb neurons are instead categorized as GABAergic interneurons (Flanigan et al., 2020; Hashikawa et al., 2020; Wallace et al., 2020). The LHb receives excitatory inputs from a wide range of limbic structures including the entopeduncular nucleus of the basal ganglia (EPN), lateral hypothalamic area (LHA), bed nucleus of the stria terminalis (BNST), and medial VTA (Lazaridis et al., 2019; Root et al., 2014; Shabel et al., 2012; Stamatakis et al., 2016). The synaptic excitation stemming from these structures onto LHb neurons governs innate and learned behaviors, thus supporting the habenular contribution to diverse motivational and cognitive functions (Lecca et al., 2017; Nuno-Perez et al., 2021; Trusel et al., 2019).

LHb neurons express α-amino-3-hydroxy-5-methyl-4-isoxazolepropionic acid receptors (AMPARs), and N-methyl-D-aspartate receptors (NMDARs) (Meye et al., 2013). The activation of glutamate receptors in the LHb results on aversive states, as concluded from paradigms of real-time place preference and foot-shock exposure (Lecca

* Corresponding author. The Department of Fundamental Neuroscience, The University of Lausanne, 1005, Lausanne, Switzerland.
** Corresponding author.
E-mail addresses: alvaro.nunoperez@unil.ch (A. Nuno-Perez), manuel.mameli@unil.ch (M. Mameli).
[1] Lead Contact

https://doi.org/10.1016/j.neuropharm.2021.108718
Received 30 April 2021; Received in revised form 12 July 2021; Accepted 13 July 2021
Available online 14 July 2021

et al., 2017; Root et al., 2014). The efficacy of AMPAR neurotransmission shapes reward-related behaviors and learning processes to anticipate punishments and negative experiences (Nuno-Perez et al., 2021; Trusel et al., 2019). Along similar lines, habenular glutamate receptors are also important in pathological contexts. The learned helplessness model of depression triggers an increase in the probability of glutamate release onto LHb synapses containing AMPARs, as well as a potentiation of AMPAR function through overexpression of the CaMKII protein (Li et al., 2011, 2013). Importantly, the same model of depression promotes burst firing of LHb neurons by activating NMDARs, and NMDAR blockade specifically in the LHb is sufficient to rescue pathological phenotypes such as anhedonia and behavioral despair (Yang et al., 2018). The latter study points to habenular NMDARs as potential targets to ameliorate symptoms of mood disorders. However, the subunit composition, biophysical properties, and synaptic plasticity rules of NMDARs in LHb neurons – especially in relation to the brain circuits in which they are embedded – remain to be studied.

NMDAR function relies on subunit composition, which can be subdivided across three different subfamilies: GluN1, GluN2A-D and GluN3A-B (Paoletti et al., 2013). Four of these subunits assemble into the core functional channel, which is permeable to sodium and calcium (Burnashev et al., 1992; Yu and Salter, 1998). NMDAR tetramers always contain two GluN1 subunits, whereas the remaining combination of GluN2 and/or GluN3 is specific to brain region, neuronal subtype, as well as cellular localization (Fritschy et al., 1998; Kumar and Huguenard, 2003; Monyer et al., 1994). Properties including single-channel conductance, Mg2+ blockade and Ca2+ permeability are under the control of subunit assembly. While, di-heteromeric GluN2A- or GluN2B-containing present high conductance and high sensitivity to Mg2+ blockade, GluN2C- or GluN2D-containing receptors have lower conductances, and sensitivity to Mg2+. Subunit composition also determines the decay kinetics of NMDA currents with GluN1/GluN2A having the fastest decay, GluN2B-containing with slower decays than GluN2A and GluN2D-containing being those receptors with the slowest kinetics Paoletti et al. (2013).

A primary function of synaptic NMDARs is ascribed to providing the calcium source for gating AMPAR adaptations (Lüscher and Malenka, 2012), but they can also undergo long-term synaptic potentiation (LTP) as shown in the CA3 region of the hippocampus and the VTA (Harnett et al., 2009; Kwon and Castillo, 2008; Rebola et al., 2008).

Here, we employed whole-cell voltage-clamp electrophysiology, optogenetic-assisted circuit mapping, and single-unit recordings in anesthetized mice to establish that (1) NMDARs contain GluN2A and/or GluN2B subunits in LHb neurons that receive glutamatergic inputs from the EPN, LHA, BNST, or medial VTA, and that (2) habenular NMDARs undergo calcium-dependent LTP following a physiologically-relevant burst protocol.

2. Materials and methods

2.1. Animals

Male mice were purchased from Janvier (C57BL6/J) and housed in groups of five per cage (4–10 weeks old). Food and water were provided *ad libitum*, and light-dark phases lasted 12 h (from 7 a.m. to 7 p.m.). All procedures aimed to fulfil the 3R criterion (replacement, reduction and refinement) and were approved by the veterinary offices of Vaud (Switzerland; license VD3171).

2.2. Stereotaxic surgeries and histology

4 weeks-old mice were anesthetized with ketamine (150 mg/kg) and xylazine (100 mg/kg) before bilateral injection of 250 nL of $rAAV_{2.5}$-hSyn1-CoChR-eGFP (titer = 1×10^{12} vg/mL) in the EPN (in mm from bregma: AP -1.2, ML ±1.8, DV -4.5), LHA (in mm from bregma: AP -1.25, ML ±1.0, DV -5.1), BNST (in mm from bregma: AP +0.3, ML ±0.9, DV -4.55), or medial VTA (in mm from bregma: AP -2, ML ±0.25, DV -4.6). Optogenetic recordings in acute brains slices were performed 3–4 weeks after stereotaxic viral injections. After recordings, slices were immersed in paraformaldehyde (4% PFA in 10 mM PBS) and kept at 4 °C until histological verification. Pictures of the injection sites were taken from the same brains that were employed for electrophysiological recordings, using an epi-fluorescent microscope (Zeiss, Germany).

2.3. Electrophysiology in acute brain slices

7-10 weeks-old mice were anesthetized with ketamine (150 mg/kg) and xylazine (100 mg/kg) prior to slice preparation. Coronal brain slices (thickness: 250 μm) containing the LHb were cut while immersed in ice-cold solution, bubbled with 95% O_2 and 5% CO_2 and containing the following reagents (in mM): Choline chloride (110); glucose (25); $NaHCO_3$ (25); $MgCl_2$ (7); ascorbic acid (11.6); sodium pyruvate (3.1); KCl (2.5); NaH_2PO_4 (1.25); and $CaCl_2$ (0.5). Slices were then allowed to recover for 1 h at room temperature in artificial cerebrospinal fluid (ACSF) containing the following reagents (in mM): NaCl (124); $NaHCO_3$ (26.2); glucose (11); KCl (2.5); $CaCl_2$ (2.5); $MgCl_2$ (1.3); and NaH_2PO_4 (1). Borosilicate glass pipettes (Phymep; impedance: 2.5–4 MΩ) were filled with CsCl-based intracellular solution containing the following reagents (in mM): CsCl (130); NaCl (4); creatine phosphate (5); $MgCl_2$ (2); Na_2ATP (2); Na_3GTP (0.6); EGTA (1.1); HEPES (5); and spermine (0.1). In the case of NMDAR and AMPAR LTP experiments, the intracellular solution was KGlu-based and contained the following reagents (in mM): KGlu (140); KCl (5); HEPES (10); EGTA (0.2); $MgCl_2$ (2); Na_2ATP (4); Na_3GTP (0.3); and creatine phosphate (10). Whole-cell voltage-clamp recordings were obtained from LHb neurons at 31 °C with a perfusion flow rate of 2.5 mL/min. Throughout recordings, the electrical signal was filtered (5 kHz) and digitized (10 kHz) using MultiClamp 200B (Molecular Devices). Data acquisition was performed with Igor Pro and NIDAQ tools (Wave Metrics). Access resistance was continuously monitored with a voltage step of −4 mV (0.1 Hz). NMDAR currents were pharmacologically isolated in the presence of the AMPAR antagonist NBQX (10 μM) and the $GABA_A$ receptor antagonist picrotoxin (100 μM). Assessment of AMPAR after the burst stimulation protocol was performed in the presence of picrotoxin (100 μM). In electrical stimulation experiments, the electrode was introduced inside a glass pipette filled with ACSF and placed within the LHb to evoke NMDAR EPSCs through an ISO-Flex stimulator coupled to a Master-8 (AMPI). For optogenetic experiments, NMDAR EPSCs were evoked with an LED coupled to an Olympus-BX51 microscope delivering pulses of blue light (Cool LED; 473 nm, ~5 mW, 1 ms). Light intensity was modulated to obtain amplitudes between 100 and 300 pA across all recordings. Neurons were clamped at +40 mV, with the exception of current-voltage relationships (from −60 mV to +40 mV, 20 mV steps) and LTP experiments (−60 mV, $MgCl_2$-free ACSF only in the case of NMDAR currents). When appropriate, the paired pulse ratio was monitored at 20 Hz. Throughout the text, TCN refers to TCN-201 and was applied to a final concentration of 10 μM (Edman et al., 2012; Stanic et al., 2015). Ifenprodil was employed at a final concentration of 5 μM (Matta et al., 2011). The decay time of NMDAR currents (tau) was calculated as the weighted time constant of two exponential functions – slow and fast – by fitting the peak-normalized EPSC from the timepoint of maximum amplitude to ≥0.8 s after (Cathala et al., 2000; Kannangara et al., 2015). Input-specific tau values were subjected to the ROUT method of outlier detection, with a maximum desired false discovery rate (Q) of 1%. This *post-hoc* analysis resulted in the detection of three outliers in the LHA and BNST datasets.

2.4. Single-unit recordings under anesthesia

10 weeks-old mice were anesthetized with intranasal isoflurane (Univentor; 2% for induction, 1–1.5% for maintenance) and placed onto a stereotaxic apparatus (Kopf Instruments). Their body temperature was

maintained at 36 °C using a feedback-controlled heating pad (CMA-450; Phymep). The scalp was retracted and a burr hole was drilled above the LHb (in mm from bregma: AP -1.32, ML ±0.42, DV -2.8), for the placement of a recording electrode. Single-unit activity of spontaneous action potentials (minimal duration of recording epochs: 3 min), was recorded extracellularly using glass micropipettes (impedance: 5–15 MΩ), filled with 2% Chicago Sky Blue dissolved in 0.5 M sodium acetate. The signal was filtered (band-pass: 500–5000 Hz), pre-amplified (DAM-80; WPI, Germany), amplified (Neurolog System; Digitimer, UK), and displayed on a digital storage oscilloscope (OX-530; Metrix, USA). Experiments were sampled online and offline by a computer connected to a laboratory interface (CED Power; Cambridge Electronic Design, UK) running the Spike2 software (Cambridge Electronic Design, UK). The burst-detection criterion was performed by qualitative analysis of inter-spike interval histograms of 200-s recordings (Lecca et al., 2017; Otsu et al., 2019). We considered a burst initiated when at least two action potentials occurred within an interval of less than 10 ms. The burst was considered to be finished when the interval between the last two action potentials was longer than 20 ms.

3. Results

3.1. Isolation of synaptic NMDAR currents in LHb neurons

We pharmacologically isolated electrically-evoked NMDAR excitatory postsynaptic currents (EPSCs) in LHb neurons by performing whole-cell voltage-clamp recordings (+40 mV) in the presence of NBQX (AMPAR antagonist, 10 μM) and picrotoxin ($GABA_A$ receptor antagonist, 100 μM). The identity of the remaining EPSC was confirmed by the sensitivity to bath application of the NMDAR antagonist amino-5-phosphonovaleric acid (APV, 100 μM) (Fig. 1A). Moreover, the pharmacologically-isolated EPSCs exhibited slow decay kinetics (Fig. 1B), which were comparable to previous reports of NMDAR currents in the hippocampus (Kannangara et al., 2015). Finally, the magnesium block of habenular NMDARs was manifested by the current rectification at negative holding potentials (Fig. 1C). Collectively, these observations indicate that our experimental settings are efficient in isolating NMDAR transmission in LHb neurons.

TCN and ifenprodil are two pharmacological agents that act as negative allosteric modulators of NMDARs containing GluN2A and GluN2B subunits, respectively (Edman et al., 2012; Matta et al., 2011). In order to study whether NMDAR assemblies in LHb neurons contain either of these subunits, we tested the NMDAR current sensitivity to these drugs. Separate bath application of TCN (10 μM) or ifenprodil (5 μM) reduced the amplitude of electrically-evoked NMDAR EPSCs (Fig. 1D and E). The combination of these compounds led to a similar reduction to the independent application of TCN and ifenprodil (Fig. 1F and G). These findings indicate that NMDAR assemblies in the LHb contain GluN2A and/or GluN2B subunits, which are likely to assemble in the form of heterotrimeric receptors.

3.2. Input-specific characterization of NMDAR transmission

LHb neurons receive glutamatergic afferents from diverse brain structures (Hu et al., 2020) hence raising the possibility that subunit composition might follow input-specific rules (Kumar and Huguenard, 2003). To investigate input-specific properties of NMDAR transmission, we independently infused a *Chloromonas oogama* channelrhodopsin (CoChR)-encoding adeno-associated virus ($AAV_{2.5}$-hSyn1-CoChR-eGFP) in the EPN, LHA, BNST, or medial VTA (Fig. 2A) (Klapoetke et al., 2014). Recording input-specific NMDAR transmission in LHb neurons revealed a reduction in EPSC amplitude upon bath application of TCN or ifenprodil, at all connections tested (Fig. 2B and C). The conserved pharmacological sensitivity of NMDAR currents prompted us to study whether the biophysical properties of these receptors were equally homogeneous across input regions. Although every connection displayed magnesium block of NMDAR transmission – as proven by the current rectification at negative holding potentials (Fig. 2D) – the degree of NMDAR rectification was smaller at BNST-to-LHb synapses compared with LHA-to-LHb and VTA-to-LHb connections (Fig. 2E). Moreover, VTA-specific NMDAR currents exhibited longer decay times than the rest of anatomical regions (Fig. 2F). Therefore, despite the differences in biophysical properties, the pharmacological results suggest that NMDAR subunit composition is comparable across synaptic inputs converging onto LHb neurons.

3.3. Synaptic plasticity of habenular NMDAR transmission

In the VTA, the pairing of presynaptic terminal stimulation with postsynaptic burst firing elicits LTP of NMDAR transmission (Harnett et al., 2009). Notably, burst firing of LHb neurons governs behavioral functions (Lecca et al., 2017; Yang et al., 2018). We thereby performed single-unit recordings in anesthetized mice with the aim of describing the burst firing properties of LHb neurons *in vivo* (Fig. 3A). The criterion for detection of burst-firing neurons was based on the qualitative analysis of their inter-spike interval histograms, as reported earlier in the habenular complex (Kowski et al., 2009; Lecca et al., 2017). This approach revealed that burst-firing neurons exhibit events of high-frequency spikes at an interval of 2–10 ms (shaded area, Fig. 3B). The intra-burst frequency of spike discharge, calculated as the ratio between the number of spikes per burst and burst duration, was approximately 200 Hz (Fig. 3C). Inspired by this property, we designed a stimulation protocol that consisted of 6 depolarizing steps (from −60 mV to 0 mV) at 200 Hz – equivalent to an epoch of 2 bursts *in vivo* – paired with a train of presynaptic stimulation (70 stimuli at 50 Hz) (Fig. 3D). The burst onset was triggered 1 s after the start of the presynaptic train, and the pairing was repeated 10 times at 0.05 Hz (Harnett et al., 2009). To study NMDAR plasticity, we performed whole-cell voltage-clamp recordings in the absence of magnesium (−60 mV). Under these conditions, the pairing protocol elicited LTP of NMDAR EPSCs (Fig. 3E). The same protocol, when applied to AMPAR EPSCs in the presence of magnesium, did not trigger LTP (Fig. 3E). Previous forms of NMDAR LTP were reported to be calcium-dependent (Harnett et al., 2009; Kwon and Castillo, 2008; Rebola et al., 2008). We hence tested whether NMDAR LTP in LHb neurons required a similar mechanism. Loading 10 mM of the calcium chelator BAPTA in the patch pipette abolished habenular NMDAR LTP (Fig. 3E). Finally, we observed that this plasticity occurred without concomitant changes in the paired pulse ratio, pointing towards a postsynaptic locus of expression (Fig. 3F).

4. Discussion

Previous studies in neocortical and hippocampal circuits revealed the input-specificity of NMDAR subunit composition through the electrical stimulation of macroscopically-segregated anatomical pathways (Carta et al., 2018; Kumar and Huguenard, 2003). However, an input-specific dissection of NMDAR assemblies in subcortical structures is missing. Here, we employed optogenetic and pharmacological methods to reveal that NMDAR subunit composition in the LHb is constant across a variety of glutamatergic inputs. Moreover, we observe that habenular NMDAR transmission is plastic following a burst protocol that combines presynaptic stimulation with postsynaptic firing.

4.1. NMDAR subunit composition in LHb neurons

GluN2A and GluN2B are the most commonly expressed NMDAR subunits in the adult brain, consistent with our findings that NMDAR currents are sensitive to TCN and ifenprodil in LHb neurons (Al-Hallaq et al., 2007; Rauner and Köhr, 2011). Despite similar sensitivity to TCN and ifenprodil across synaptic inputs onto LHb neurons, NMDAR EPSCs at VTA-to-LHb synapses presented the slowest decay kinetics. This contrasts with recent findings where LHA-evoked NMDAR EPSCs

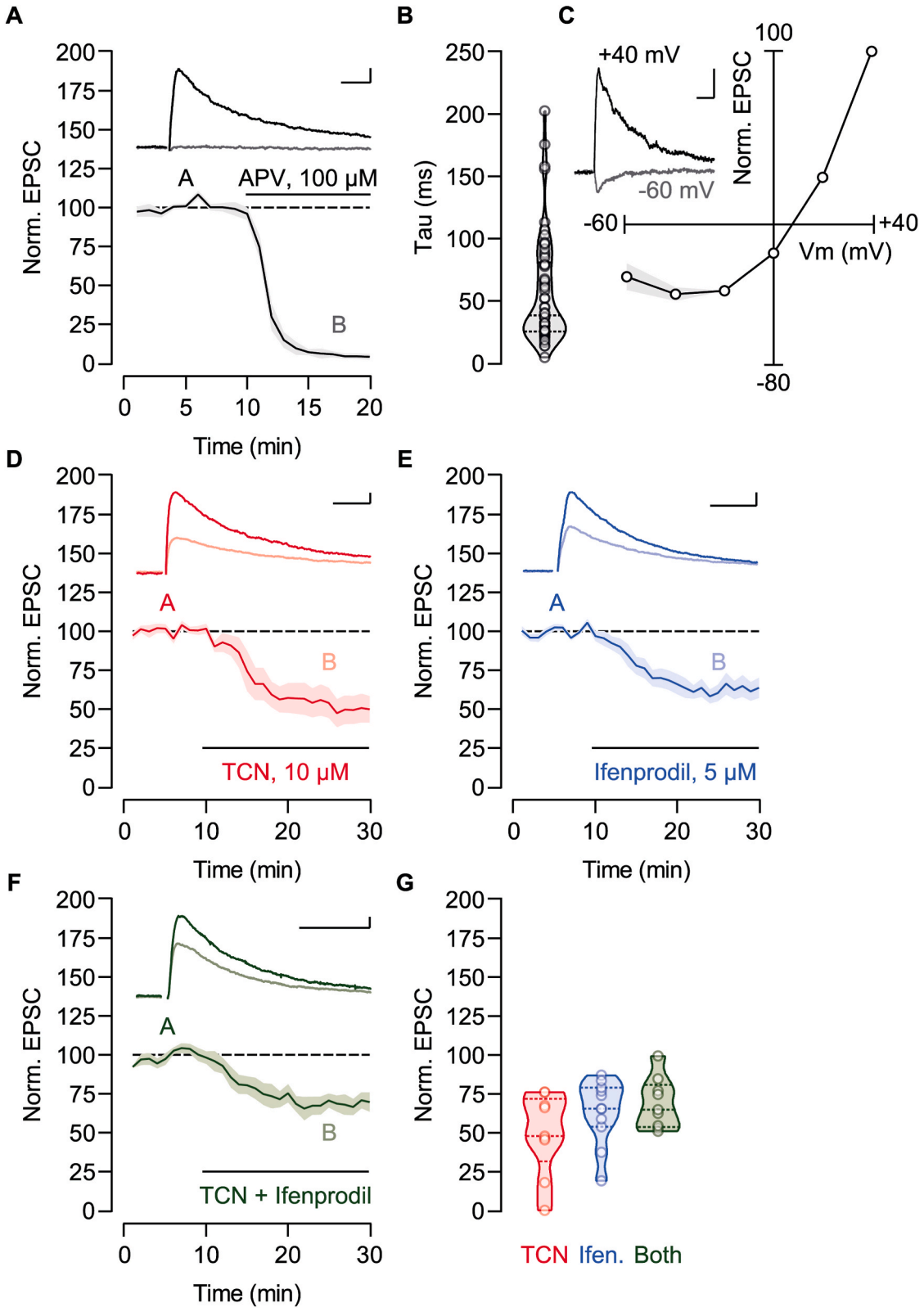

Fig. 1. Isolation of synaptic NMDAR currents in LHb neurons. (A) Example traces (scale bars: 20 pA and 20 ms) and time course of normalized NMDAR-EPSC amplitudes before (black, A) and after (grey, B) APV application (n = 2 mice/10 cells). **(B)** Violin and scatter plots of NMDAR-EPSC decay time (n = 12 mice/58 cells, 55.3 ± 5.6 ms). **(C)** Example traces (scale bars: 20 pA and 20 ms) and current-voltage relationship of normalized NMDAR-EPSC amplitudes (n = 4 mice/28 cells). **(D)** Example traces (scale bars: 20 pA and 20 ms) and time course of normalized NMDAR-EPSC amplitudes before (dark red, A) and after (light red, B) TCN application (n = 3 mice/9 cells). **(E)** Example traces (scale bars: 20 pA and 20 ms) and time course of normalized NMDAR-EPSC amplitudes before (dark blue, A) and after (light blue, B) ifenprodil application (n = 3 mice/11 cells). **(F)** Example traces (scale bars: 20 pA and 20 ms) and time course of normalized NMDAR-EPSC amplitudes before (dark green, A) and after (light green, B) TCN and ifenprodil application (n = 2 mice/9 cells). **(G)** Violin and scatter plots of normalized NMDAR-EPSC amplitudes during the last 5 min of the recordings (49.4 ± 8.7% for TCN, 63.8 ± 6.2% for ifenprodil, and 69.1 ± 5.4% for TCN and ifenprodil).

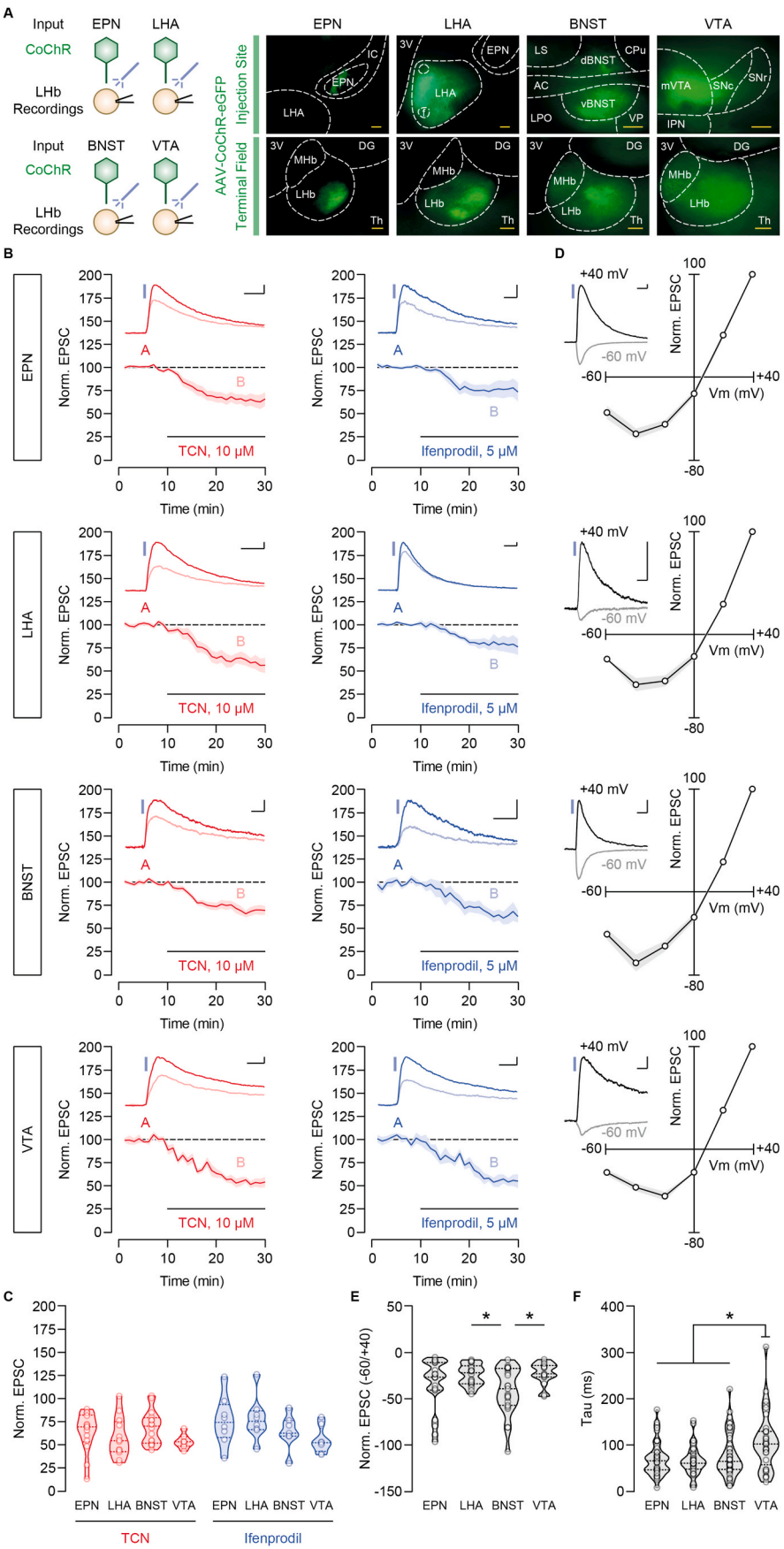

Fig. 2. Input-specific characterization of NMDAR transmission. (A) Schematic of the experimental design. Representative injection sites of AAV-CoChR (top, scale bar: 200 μm) and the corresponding terminal field within the LHb (bottom, scale bar: 100 μm). AC, anterior commissure; CPu, caudate putamen; d/vBNST, dorsal/ventral bed nucleus of the stria terminalis; DG, dentate gyrus; EPN, entopeduncular nucleus; f, fornix; 3V, third ventricle; IC, internal capsule; IPN, interpeduncular nucleus; LHA, lateral hypothalamic area; LPO, lateral preoptic area; LS, lateral septum; M/LHb, medial/lateral habenula; mVTA, medial ventral tegmental area; SNr/c, substantia nigra pars reticulata/compacta; Th, thalamus; VP, ventral pallidum. **(B)** Example traces (scale bars: 20 pA and 20 ms) and time courses of normalized NMDAR-EPSC amplitudes before (dark red, A) and after (light red, B) TCN application (EPN: n = 8 mice/14 cells; LHA: n = 6 mice/12 cells; BNST: n = 6 mice/16 cells; VTA: n = 2 mice/7 cells). Example traces (scale bars: 20 pA and 20 ms) and time courses of normalized NMDAR-EPSC amplitudes before (dark blue, A) and after (light blue, B) ifenprodil application (EPN: n = 4 mice/8 cells; LHA: n = 3 mice/8 cells; BNST: n = 3 mice/7 cells; VTA: n = 2 mice/8 cells). **(C)** Violin and scatter plots of normalized NMDAR-EPSC amplitudes during the last 5 min of the recordings across input regions (EPN: 63.8 ± 5.8% for TCN and 76 ± 9.5% for ifenprodil; LHA: 58.3 ± 6.4% for TCN and 78.4 ± 8.2% for ifenprodil; BNST: 68.8 ± 4.5% for TCN and 64.1 ± 7.1% for ifenprodil; VTA: 53.7 ± 2.9% for TCN and 55.1 ± 5.1% for ifenprodil). **(D)** Example traces (scale bars: 50 pA and 20 ms) and current-voltage relationships of normalized NMDAR-EPSC amplitudes across input regions (EPN: n = 4 mice/23 cells; LHA: n = 3 mice/20 cells; BNST: n = 3 mice/26 cells; VTA: n = 5 mice/18 cells). **(E)** Violin and scatter plots of NMDAR-EPSC inward rectification across input regions (EPN: n = 4 mice/20 cells, −34.6 ± 6.3%; LHA: n = 3 mice/20 cells, −24.2 ± 2.5%; BNST: n = 3 mice/23 cells, −41.4 ± 5.3%; VTA: n = 5 mice/15 cells, −22.7 ± 3.1%). One-way ANOVA ($F_{3,74}$ = 3.7) with Dunnett correction (*p < 0.05). **(F)** Violin and scatter plots of NMDAR-EPSC decay time across input regions (EPN: n = 16 mice/45 cells, 70.4 ± 5.4 ms; LHA: n = 12 mice/35 cells, 66 ± 5.4 ms; BNST: n = 12 mice/46 cells, 77.5 ± 6.9 ms; VTA: n = 9 mice/33 cells, 107.2 ± 10.8 ms). One-way ANOVA ($F_{3,155}$ = 3.1) with Dunnett correction (*p < 0.05).

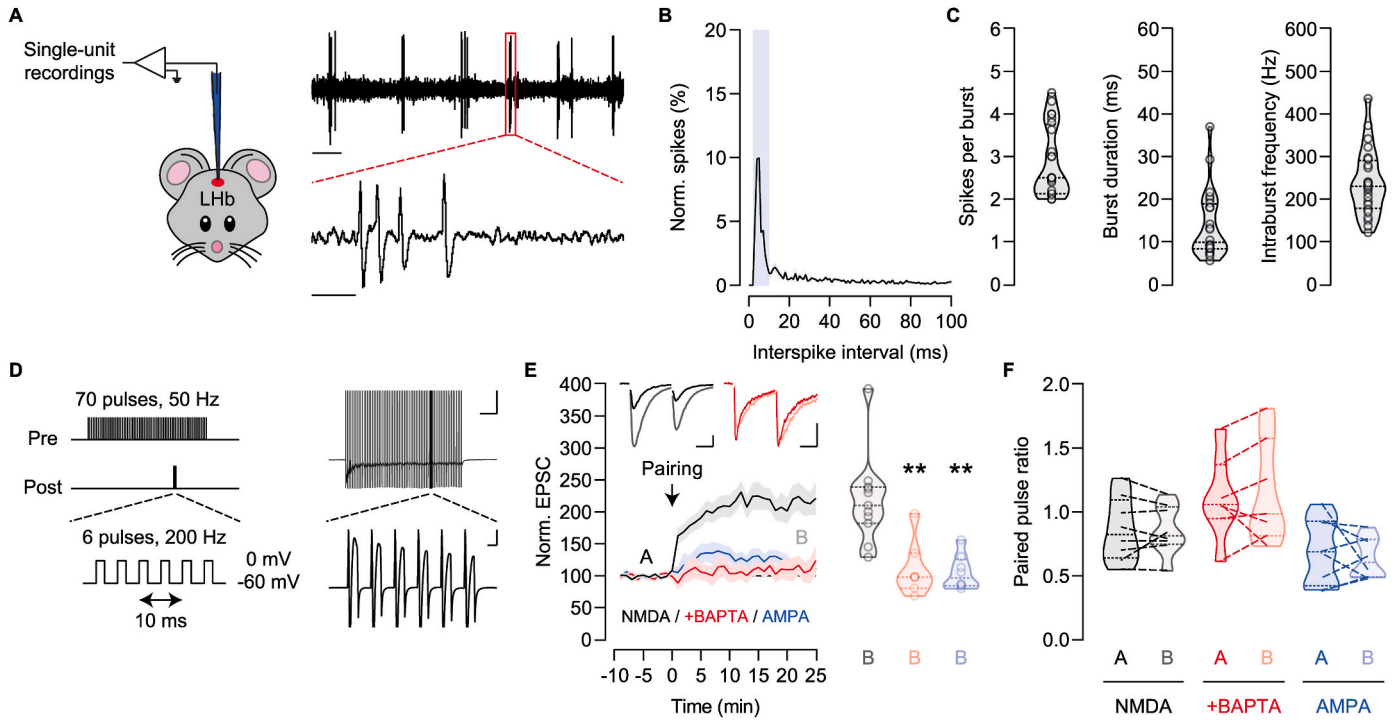

Fig. 3. Synaptic plasticity of habenular NMDAR transmission. (A) Schematic of the experimental approach. Example traces of spontaneous firing activity in the LHb (scale bars: 500 ms for upper trace, 10 ms for lower trace). **(B)** Histogram depicting the detection probability of spikes within a certain inter-spike interval in burst-firing neurons (n = 3 mice/13 cells). The blue-shaded area highlights an interval range of 2–10 ms. **(C)** Violin and scatter plots of burst properties in all neurons recorded (n = 3 mice/24 cells, 2.9 ± 0.2 spikes per burst, 13.8 ± 1.6 ms and 238.8 ± 15.8 Hz). **(D)** Schematic and example traces of the plasticity protocol (scale bars: 200 ms and 200 pA for upper trace, 2 ms and 500 pA for lower trace). **(E)** Example traces (scale bars: 20 pA and 20 ms) and time course of normalized NMDAR-EPSC amplitudes before (A) and after (B) the plasticity protocol in control conditions (black, n = 7 mice/11 cells) and in the presence of BAPTA (red, n = 5 mice/7 cells). Time course of normalized AMPAR-EPSC amplitudes before (A) and after (B) the plasticity protocol (blue, n = 2 mice/8 cells). Violin and scatter plots of normalized EPSC amplitudes during the last 5 min of the recordings (218.7 ± 20.9% for NMDA, 110.9 ± 16.5% for NMDA + BAPTA, and 105.4 ± 9.5% for AMPA). One-way ANOVA ($F_{2,\ 23} = 13.9$) with Dunnett correction (**p < 0.001). **(F)** Violin and scatter plots of NMDA paired pulse ratio in control conditions (black, n = 5 mice/8 cells, 0.85 ± 0.09 for A and 0.85 ± 0.07 for B) and in the presence of BAPTA (red, n = mice/cells, 1.1 ± 0.12 for A and 1.15 ± 0.15 for B). Violin and scatter plots of AMPA paired pulse ratio (blue, n = 2 mice/8 cells, 0.71 ± 0.09 for A and 0.65 ± 0.06 for B).

exhibited the largest decay time (Cerniauskas et al., 2019). A major difference among the two studies is the presence or absence of the identification of LHb projection targets. It is plausible that neurons receiving similar inputs, but projecting to different anatomical structures, may present distinct synaptic properties.

Furthermore, our data do not rule out additional constituents of habenular NMDAR assemblies. Neurons in the neighboring medial habenula, which shares a common ontogeny with the LHb, express GluN3A subunits (Otsu et al., 2019; Schmidt and Pasterkamp, 2017). These subunits generate NMDARs with the ability to be gated purely by glycine, in the absence of glutamate, potentially making an impact on neuronal plasticity processes (Grand et al., 2018). However, given the limited specificity of GluN3A-directed pharmacology, a genetic approach would be more suitable to assess whether LHb NMDARs also contain functional GluN3A subunits (Creed et al., 2016; Otsu et al., 2019).

An interesting feature of the NMDAR subunit composition reported here is the lack of input specificity. This opens the possibility that the region-specific differences in current-voltage relationship, magnesium sensitivity, and decay time of NMDAR currents might result from additional factors, including alternative landscapes of postsynaptic anchoring proteins (Bard et al., 2010; Ferreira et al., 2015). This is likely the case in light of the large variability of NMDAR pharmacological sensitivity observed across diverse synaptic inputs. In addition to differences in scaffolding assemblies, morphology and input-output connectivity might also contribute to the observed variance (Cerniauskas et al., 2019; Lecca et al., 2017).

4.2. Implications of NMDAR subunit composition for habenular AMPAR plasticity

One of the principal functions of NMDAR transmission throughout the brain is to provide the calcium source required to gate AMPAR adaptations (Lüscher and Malenka, 2012). For example, while synapses in the hippocampal CA3 region lack the ability to undergo AMPAR LTP under basal conditions, an increase in NMDAR levels unmasks this plasticity (Rebola et al., 2011). In this regard, NMDAR subunit composition determines whether NMDAR-dependent calcium influx leads to AMPAR LTP or long-term depression (LTD). Indeed, GluN2A subunits are necessary for AMPAR LTP, while their GluN2B counterparts are instead required for LTD (Brigman et al., 2010). This is interesting from an habenular perspective, since NMDAR transmission gates AMPAR LTP and LTD in LHb neurons (Trusel et al., 2019). This supports the conserved contribution of GluN2A and GluN2B subunits for the induction of NMDAR-dependent LTP and LTD, respectively, across cortical and subcortical structures (Shipton and Paulsen, 2014).

4.3. Cellular substrates for habenular NMDAR plasticity

Our data indicate that NMDAR transmission in LHb neurons undergoes synaptic plasticity. Accordingly, NMDAR LTP can be elicited by driving a presynaptic tetanus in the hippocampus (Kwon and Castillo, 2008; Rebola et al., 2008). In VTA neurons, NMDAR potentiation requires instead the pairing of presynaptic stimulation with postsynaptic firing (Harnett et al., 2009). Our study describes an *in vivo*-based burst protocol, capable of potentiating NMDAR transmission, that also

requires the coincident detection of a presynaptic train with post-synaptic bursts of activity. Although this protocol mimics LHb neuronal firing, we designed its duration based on published literature (Kwon and Castillo, 2008; Rebola et al., 2008; Harnett et al., 2009). However, the physiological validity of such duration remains to be addressed *in vivo*.

The LTP of habenular NMDAR transmission requires a raise in intracellular calcium. Although not identified in this study, the source of calcium might be metabotropic glutamate receptors, in line with previous observations in the hippocampus and VTA (Harnett et al., 2009; Kwon and Castillo, 2008; Rebola et al., 2008). Such receptors are expressed in LHb neurons and mediate synaptic adaptations (Valentinova and Mameli, 2016). Future studies will need to determine the signaling cascade underlying the synaptic plasticity described here.

Habenular AMPARs undergo synaptic plasticity in diverse behavioral contexts (Li et al., 2011, 2013). The fact that NMDARs are plastic *ex vivo* opens the possibility that behavioral experience might as well alter NMDAR transmission *in vivo*. This is relevant when analyzing electrophysiological markers like AMPA:NMDA ratio, and highlights the need for a thorough assessment of which component is adapting during experience-driven plasticity.

4.4. Implications of NMDAR plasticity for mental health

The burst properties of our pairing protocol in acute brain slices aim to mimic the firing modality of LHb neurons *in vivo*. The detection of burst activity is in line with published evidence obtained in the LHb of anesthetized rodents (Kowski et al., 2009; Lecca et al., 2017). These data suggest the potential role that burst-driven LTP of habenular NMDAR transmission may have in behaviorally-relevant contexts. Along these lines, NMDAR transmission is engaged in the chronic restraint stress and learned helplessness models of depression, leading to increased burst firing of LHb neurons (Cui et al., 2018; Yang et al., 2018). These observations support a scenario in which NMDAR transmission can be potentiated under pathological conditions, as a result of increased burst activity, potentially occluding the habenular NMDAR LTP described here. The opposite situation could also apply. Schizophrenia – an alternative neuropsychiatric disorder linked to LHb dysfunction (Shepard et al., 2006) – is rather associated with the hypofunction of NMDAR transmission (Belforte et al., 2010). Therefore, the activity-dependent plasticity of habenular NMDAR synapses may have different roles depending on the pathological phenotype.

5. Conclusions

Collectively, our findings describe the biophysical and synaptic properties of NMDAR transmission in LHb neurons. These observations might prove useful to study NMDAR plasticity in experience-dependent contexts, and to finetune NMDAR-directed pharmacological targets in preclinical models linking LHb dysfunction to neuropsychiatric disorders.

CRediT authorship contribution statement

Alvaro Nuno-Perez: experiment design, writing the manuscript, *in vitro* experiments and data analysis. Sarah Mondoloni: *in vitro* experiments and data analysis. Anna Tchenio: *in vitro* experiments. Salvatore Lecca: *in vivo* experiments and data analysis. Manuel Mameli: experiment design, supervision, editing and writing the manuscript.

Declaration of competing interest

The authors declare that the research was conducted in the absence of any commercial or financial relationships that could be construed as a potential conflict of interest.

Acknowledgements

We thank all members from the Mameli Laboratory for discussion and feedback on the work. This study was supported by grants to Manuel Mameli from the Swiss National Science Foundation (31003A_175549).

References

Al-Hallaq, R.A., Conrads, T.P., Veenstra, T.D., Wenthold, R.J., 2007. NMDA di-heteromeric receptor populations and associated proteins in rat hippocampus. J. Neurosci. 27, 8334–8343.

Bard, L., Sainlos, M., Bouchet, D., Cousins, S., Mikasova, L., Breillat, C., Stephenson, F.A., Imperiali, B., Choquet, D., Groc, L., 2010. Dynamic and specific interaction between synaptic NR2-NMDA receptor and PDZ proteins. Proc. Natl. Acad. Sci. U. S. A. 107, 19561–19566.

Belforte, J.E., Zsiros, V., Sklar, E.R., Jiang, Z., Yu, G., Li, Y., Quinlan, E.M., Nakazawa, K., 2010. Postnatal NMDA receptor ablation in corticolimbic interneurons confers schizophrenia-like phenotypes. Nat. Neurosci. 13, 76–83.

Bianco, I.H., Wilson, S.W., 2009. The habenular nuclei: a conserved asymmetric relay station in the vertebrate brain. Philos. Trans. R. Soc. Lond. B Biol. Sci. 364, 1005–1020.

Brigman, J.L., Wright, T., Talani, G., Prasad-Mulcare, S., Jinde, S., Seabold, G.K., Mathur, P., Davis, M.I., Bock, R., Gustin, R.M., Colbran, R.J., Alvarez, V.A., Nakazawa, K., Delpire, E., Lovinger, D.M., Holmes, A., 2010. Loss of GluN2B-containing NMDA receptors in CA1 hippocampus and cortex impairs long-term depression, reduces dendritic spine density, and disrupts learning. J. Neurosci. 31, 4590–4600.

Burnashev, N., Schoepfer, R., Monyer, H., Ruppersberg, J.P., Günther, W., Seeburg, P.H., Sakmann, B., 1992. Control by asparagine residues of calcium permeability and magnesium blockade in the NMDA receptor. Science 257, 1415–1419.

Carta, M., Srikumar, B.N., Gorlewicz, A., Rebola, N., Mulle, C., 2018. Activity-dependent control of NMDA receptor subunit composition at hippocampal mossy fibre synapses. J. Physiol. 596, 703–716.

Cathala, L., Misra, C., Cull-Candy, S., 2000. Developmental profile of the changing properties of NMDA receptors at cerebellar mossy fiber-granule cell synapses. J. Neurosci. 20, 5899–5905.

Cerniauskas, I., Winterer, J., de Jong, J.W., Lukacsovich, D., Yang, H., Khan, F., Peck, J. R., Obayashi, S.K., Lilascharoen, V., Lim, B.K., Földy, C., Lammel, S., 2019. Chronic stress induces activity, synaptic, and transcriptional remodeling of the lateral habenula associated with deficits in motivated behaviors. Neuron 104, 899–915.

Clerke, J., Preston-Ferrer, P., Zouridis, I.S., Tissot, A., Batti, L., Voigt, F.F., Pagès, S., Burgalossi, A., Mameli, M., 2021. Output-specific adaptation of habenula-midbrain excitatory synapses during cocaine withdrawal. Front. Synaptic Neurosci. 13, 643138.

Creed, M., Kaufling, J., Fois, G.R., Jalabert, M., Yuan, T., Lüscher, C., Georges, F., Bellone, C., 2016. Cocaine exposure enhances the activity of ventral tegmental area dopamine neurons via calcium-impermeable NMDARs. J. Neurosci. 36, 10759–10768.

Cui, Y., Yang, Y., Ni, Z., Dong, Y., Cai, G., Foncelle, A., Ma, S., Sang, K., Tang, S., Li, Y., Shen, Y., Berry, H., Wu, S., Hu, H., 2018. Astroglial Kir4.1 in the lateral habenula drives neuronal bursts in depression. Nature 554, 323–327.

Edman, S., McKay, S., Macdonald, L.J., Samadi, M., Livesey, M.R., Hardingham, G.E., Wyllie, D.J., 2012. TCN 201 selectively blocks GluN2A-containing NMDARs in a GluN1 co-agonist dependent but non-competitive manner. Neuropharmacology 63, 441–449.

Ferreira, J.S., Schmidt, J., Rio, P., Águas, R., Rooyakkers, A., Li, K.W., Smit, A.B., Craig, A.M., Carvalho, A.L., 2015. GluN2B-Containing NMDA receptors regulate AMPA receptor traffic through anchoring of the synaptic proteasome. J. Neurosci. 35, 8462–8479.

Flanigan, M.E., Aleyasin, H., Li, L., Burnett, C.J., Chan, K.L., LeClair, K.B., Lucas, E.K., Matikainen-Ankney, B., Durand-de Cuttoli, R., Takahashi, A., Menard, C., Pfau, M.L., Golden, S.A., Bouchard, S., Calipari, E.S., Nestler, E.J., DiLeone, R.J., Yamanaka, A., Huntley, G.W., Clem, R.L., Russo, S.J., 2020. Orexin signaling in GABAergic lateral habenula neurons modulates aggressive behavior in male mice. Nat. Neurosci. 23, 638–650.

Fritschy, J.M., Weinmann, O., Wenzel, A., Benke, D., 1998. Synapse-specific localization of NMDA and GABA(A) receptor subunits revealed by antigen-retrieval immunohistochemistry. J. Comp. Neurol. 390, 194–210.

Grand, T., Abi Gerges, S., David, M., Diana, M.A., Paoletti, P., 2018. Unmasking GluN1/GluN3A excitatory glycine NMDA receptors. Nat. Commun. 9, 4769.

Harnett, M.T., Bernier, B.E., Ahn, K.C., Morikawa, H., 2009. Burst-timing-dependent plasticity of NMDA receptor-mediated transmission in midbrain dopamine neurons. Neuron 62, 826–838.

Hashikawa, Y., Hashikawa, K., Rossi, M.A., Basiri, M.L., Liu, Y., Johnston, N.L., Ahmad, O.R., Stuber, G.D., 2020. Transcriptional and spatial resolution of cell types in the mammalian habenula. Neuron 106, 743–758.

Hu, H., Cui, Y., Yang, Y., 2020 May. Circuits and functions of the lateral habenula in health and in disease. Nat. Rev. Neurosci. 21 (5), 277–295. https://doi.org/10.1038/s41583-020-0292-4. Epub 2020 Apr 8. PMID: 32269316.

Kannangara, T.S., Eadie, B.D., Bostrom, C.A., Morch, K., Brocardo, P.S., Christie, B.R., 2015. GluN2A-/- mice lack bidirectional synaptic plasticity in the dentate gyrus and perform poorly on spatial pattern separation tasks. Cerebr. Cortex 25, 2102–2113.

Klapoetke, N.C., Murata, Y., Kim, S.S., Pulver, S.R., Birdsey-Benson, A., Cho, Y.K., Morimoto, T.K., Chuong, A.S., Carpenter, E.J., Tian, Z., Wang, J., Xie, Y., Yan, Z.,

Zhang, Y., Chow, B.Y., Surek, B., Melkonian, M., Jayaraman, V., Constantine-Paton, M., Wong, G.K., Boyden, E.S., 2014. Independent optical excitation of distinct neural populations. Nat. Methods 11, 338–346.
Kowski, A.B., Veh, R.W., Weiss, T., 2009. Dopaminergic activation excites rat lateral habenular neurons in vivo. Neuroscience 161, 1154–1165.
Kumar, S.S., Huguenard, J.R., 2003. Pathway-specific differences in subunit composition of synaptic NMDA receptors on pyramidal neurons in neocortex. J. Neurosci. 23, 10074–10083.
Kwon, H.B., Castillo, P.E., 2008. Long-term potentiation selectively expressed by NMDA receptors at hippocampal mossy fiber synapses. Neuron 57, 108–120.
Lazaridis, I., Tzortzi, O., Weglage, M., Märtin, A., Xuan, Y., Parent, M., Johansson, Y., Fuzik, J., Fürth, D., Fenno, L.E., Ramakrishnan, C., Silberberg, G., Deisseroth, K., Carlén, M., Meletis, K., 2019. A hypothalamus-habenula circuit controls aversion. Mol. Psychiatr. 24, 1351–1368.
Lecca, S., Meye, F.J., Trusel, M., Tchenio, A., Harris, J., Schwarz, M.K., Burdakov, D., Georges, F., Mameli, M., 2017. Aversive stimuli drive hypothalamus-to-habenula excitation to promote escape behavior. Elife 6.
Li, B., Piriz, J., Mirrione, M., Chung, C., Proulx, C.D., Schulz, D., Henn, F., Malinow, R., 2011. Synaptic potentiation onto habenula neurons in the learned helplessness model of depression. Nature 470, 535–539.
Li, K., Zhou, T., Liao, L., Yang, Z., Wong, C., Henn, F., Malinow, R., Yates, J.R., Hu, H., 2013. βCaMKII in lateral habenula mediates core symptoms of depression. Science 341, 1016–1020.
Lüscher, C., Malenka, R.C., 2012. NMDA receptor-dependent long-term potentiation and long-term depression (LTP/LTD). Cold Spring Harb Perspect Biol 4.
Matsumoto, M., Hikosaka, O., 2007. Lateral habenula as a source of negative reward signals in dopamine neurons. Nature 447, 1111–1115.
Matta, J.A., Ashby, M.C., Sanz-Clemente, A., Roche, K.W., Isaac, J.T., 2011. mGluR5 and NMDA receptors drive the experience- and activity-dependent NMDA receptor NR2B to NR2A subunit switch. Neuron 70, 339–351.
Meye, F.J., Lecca, S., Valentinova, K., Mameli, M., 2013. Synaptic and cellular profile of neurons in the lateral habenula. Front. Hum. Neurosci. 7, 860.
Monyer, H., Burnashev, N., Laurie, D.J., Sakmann, B., Seeburg, P.H., 1994. Developmental and regional expression in the rat brain and functional properties of four NMDA receptors. Neuron 12, 529–540.
Nuno-Perez, A., Trusel, M., Lalive, A.L., Congiu, M., Gastaldo, D., Tchenio, A., Lecca, S., Soiza-Reilly, M., Bagni, C., Mameli, M., 2021. Stress undermines reward-guided cognitive performance through synaptic depression in the lateral habenula. Neuron 109, 947–956.
Otsu, Y., Darcq, E., Pietrajtis, K., Mátyás, F., Schwartz, E., Bessaih, T., Abi Gerges, S., Rousseau, C.V., Grand, T., Dieudonné, S., Paoletti, P., Acsády, L., Agulhon, C., Kieffer, B.L., Diana, M.A., 2019. Control of aversion by glycine-gated GluN1/GluN3A NMDA receptors in the adult medial habenula. Science 366, 250–254.
Paoletti, P., Bellone, C., Zhou, Q., 2013. NMDA receptor subunit diversity: impact on receptor properties, synaptic plasticity and disease. Nat. Rev. Neurosci. 14, 383–400.
Rauner, C., Köhr, G., 2011. Triheteromeric NR1/NR2A/NR2B receptors constitute the major N-methyl-D-aspartate receptor population in adult hippocampal synapses. J. Biol. Chem. 286, 7558–7566.
Rebola, N., Carta, M., Lanore, F., Blanchet, C., Mulle, C., 2011. NMDA receptor-dependent metaplasticity at hippocampal mossy fiber synapses. Nat. Neurosci. 14, 691–693.
Rebola, N., Lujan, R., Cunha, R.A., Mulle, C., 2008. Adenosine A2A receptors are essential for long-term potentiation of NMDA-EPSCs at hippocampal mossy fiber synapses. Neuron 57, 121–134.
Root, D.H., Mejias-Aponte, C.A., Zhang, S., Wang, H.L., Hoffman, A.F., Lupica, C.R., Morales, M., 2014. Single rodent mesohabenular axons release glutamate and GABA. Nat. Neurosci. 17, 1543–1551.
Schmidt, E.R.E., Pasterkamp, R.J., 2017. The molecular mechanisms controlling morphogenesis and wiring of the habenula. Pharmacol. Biochem. Behav. 162, 29–37.
Shabel, S.J., Proulx, C.D., Trias, A., Murphy, R.T., Malinow, R., 2012. Input to the lateral habenula from the basal ganglia is excitatory, aversive, and suppressed by serotonin. Neuron 74, 475–481.
Shepard, P.D., Holcomb, H.H., Gold, J.M., 2006. Schizophrenia in translation: the presence of absence: habenular regulation of dopamine neurons and the encoding of negative outcomes. Schizophr. Bull. 32, 417–421.
Shipton, O.A., Paulsen, O., 2014. GluN2A and GluN2B subunit-containing NMDA receptors in hippocampal plasticity. Philos. Trans. R. Soc. Lond. B Biol. Sci. 369.
Stamatakis, A.M., Van Swieten, M., Basiri, M.L., Blair, G.A., Kantak, P., Stuber, G.D., 2016. Lateral hypothalamic area glutamatergic neurons and their projections to the lateral habenula regulate feeding and reward. J. Neurosci. 36, 302–311.
Stanic, J., Carta, M., Eberini, I., Pelucchi, S., Marcello, E., Genazzani, A.A., Racca, C., Mulle, C., Di Luca, M., Gardoni, F., 2015. Rabphilin 3A retains NMDA receptors at synaptic sites through interaction with GluN2A/PSD-95 complex. Nat. Commun. 6, 10181.
Stern, W.C., Johnson, A., Bronzino, J.D., Morgane, P.J., 1979. Effects of electrical stimulation of the lateral habenula on single-unit activity of raphe neurons. Exp. Neurol. 65, 326–342.
Trusel, M., Nuno-Perez, A., Lecca, S., Harada, H., Lalive, A.L., Congiu, M., Takemoto, K., Takahashi, T., Ferraguti, F., Mameli, M., 2019. Punishment-predictive cues guide avoidance through potentiation of hypothalamus-to-habenula synapses. Neuron 102, 120–127.
Valentinova, K., Mameli, M., 2016. mGluR-LTD at excitatory and inhibitory synapses in the lateral habenula tunes neuronal output. Cell Rep. 16, 2298–2307.
Wallace, M.L., Huang, K.W., Hochbaum, D., Hyun, M., Radeljic, G., Sabatini, B.L., 2020. Anatomical and single-cell transcriptional profiling of the murine habenular complex. Elife 9.
Yang, Y., Cui, Y., Sang, K., Dong, Y., Ni, Z., Ma, S., Hu, H., 2018. Ketamine blocks bursting in the lateral habenula to rapidly relieve depression. Nature 554, 317–322.
Yu, X.M., Salter, M.W., 1998. Gain control of NMDA-receptor currents by intracellular sodium. Nature 396, 469–474.